Flexibility of End-Labeled Polymers from Electron Spin Resonance Line-Shape Analysis: 3′ Terminus of Transfer Ribonucleic Acid and 5S Ribonucleic Acid†

Greg A. Luoma, F. Geoffrey Herring,* and Alan G. Marshall*

ABSTRACT: *Saccharomyces cerevisiae* tRNA and 5S RNA, *Escherichia coli* 5S RNA, and wheat germ 5S RNA have each been specifically spin-labeled at the 3′-terminal ribose to give morpholino-spin-labeled (MSL) RNAs. Enzymatic hydrolysis with pancreatic RNase, followed by anion-exchange chromatography, confirms the site of attachment of the spin-label. Effective rotational correlation times, τ_B and τ_C, have been determined from electron spin resonance (ESR) peak heights and widths as a function of temperature for each MSL RNA, and Arrhenius plots of $-\log \tau$ vs. $1/T$ have been constructed. τ_C is a measure of internal flexibility at the link between the label and the RNA, while τ_B is a measure of rotational flexibility of the RNA near the labeled site. Validity of the τ_B and τ_C determination has been confirmed from simulation of the experimental EPR spectra by theoretical spectra computed for various attachment geometries and motional rates. Discontinuities in the slope of Arrhenius plots for τ_B were seen at 34 and 66 °C (yeast MSL tRNA), 37 and 60 °C (*E. coli* MSL 5S RNA), 37 and 57 °C (yeast MSL 5S RNA), and 36 and 54 °C (wheat germ MSL 5S RNA). Temperature-induced hydrolysis of each MSL RNA was less than 5% as determined by gel-filtration chromatography. The melting curves are consistent with a recently proposed universal secondary structural model for prokaryotic and eukaryotic 5S RNA.

New generalized secondary structures for eukaryotic 5S RNA and 5.8S RNA and prokaryotic 5S RNA have recently been proposed (Luoma & Marshall, 1978a,b). The new structures can be adapted to every one of the known 5S RNA nucleotide sequences (Luoma & Marshall, 1978b; Luoma et al., 1980; Burns et al., 1980; G. A. Luoma and A. G. Marshall, unpublished results). These small RNA molecules are thought to participate in binding tRNA to the ribosome during protein synthesis (Erdmann, 1976; Swartz et al., 1976). In prokaryotes, 5S RNA contains a constant CGAAC segment (positions 40–45 of 5S RNA). In eukaryotes, an analogous GAUC segment (and thus presumably the analogous function) is found for 5.8S RNA (Erdmann, 1978).

Interpretation of the many experimentally determined spectroscopic properties and chemical reactivities of tRNA molecules (Reid, 1981; Rich & RajBhandary, 1976; Robertus et al., 1974; Chen et al., 1975) has been advanced markedly by the recent solution of the crystal and molecular structure of yeast $tRNA^{Phe}$ by X-ray diffraction (Rich & Kim, 1978; Hingerty et al., 1978). Furthermore, since recently proposed secondary structural models for eukaryotic and prokaryotic 5S RNA exhibit "stem" and "loop" regions disposed in a cloverleaf highly analogous to that in tRNA (Rich & Kim, 1978; Hingerty et al., 1978; Holley et al., 1965), many structural properties of the 5S RNA and 5.8S RNA molecules may be deduced by comparison to measurements made on tRNA (Luoma & Marshall, 1978a,b; Luoma et al., 1980; Burns et al., 1980; G. A. Luoma and A. G. Marshall, unpublished results).

A variety of physical and chemical measurements in solution, summarized in two recent reviews (Erdmann, 1976; Monier, 1974), largely support a cloverleaf secondary structure for 5S RNA, as do more recent enzymatic digestion (Barber & Nichols, 1978; Vigne & Jordan, 1977), Raman (Chen et al., 1978), nuclear magnetic resonance (NMR) (Marshall & Smith, 1977, 1980; Hamill et al., 1980), low-angle X-ray scattering (Osterberg et al., 1976), infrared (Appel et al., 1979; Stulz et al., 1981), optical (Burns et al., 1980), tritium exchange (Ramstein & Erdmann, 1981), and chemical cross-linking data (Wagner & Garrett, 1978). In addition, changes in circular dichroism (Willick et al., 1978; Bear et al., 1977; Fox & Wong, 1978) and oligonucleotide binding (Erdmann, 1976) on combination of particular ribosomal proteins with 5S RNA strongly suggest that some ribosomal proteins appear to change the structure of 5S RNA on binding. In order to establish a secondary structure for free 5S RNA and to monitor changes in that structure on interaction with other ribosomal components, it is necessary to use a spectroscopic structural probe applicable to dilute solutions.

An increasingly popular approach for establishing the relative thermodynamic or motional stabilities of various secondary and tertiary structural segments of macromolecules in solution is to monitor the sequential unfolding of the macromolecule as a function of the increase in temperature or change in concentration of denaturants. For small RNAs (tRNA, 5S RNA, 5.8S RNA) in the presence of sufficient (ca. 10 mM) Mg^{2+} to ensure a native conformation at low temperatures, it has proved difficult to resolve different temperature-induced structural unfolding stages by UV absorption (Fiesner & Maass, 1973) or differential scanning calorimetry (Privalov et al., 1975) techniques. With those techniques, it is necessary to remove the Mg^{2+} (thereby denaturing the RNA even at low temperature) in order to decrease the unfolding temperatures of the less stable structural segments sufficiently to resolve them from the unfolding of the more stable segments.

† From the Defence Research Establishment Pacific, Department of National Defence, FMO Esquimalt, British Columbia V05 1B0, Canada (G.A.L.), the Department of Chemistry, University of British Columbia, Vancouver, British Columbia V6T 1Y6, Canada (F.G.H.), and the Departments of Chemistry and Biochemistry, The Ohio State University, Columbus, Ohio 43210 (A.G.M.). *Received February 4, 1982; revised manuscript received August 4, 1982.* Supported by grants from the Natural Sciences and Engineering Research Council of Canada (F.G.H. and A.G.M.), the U.S. Public Health Service (A.G.M., National Institutes of Health Grant GM-29274), and the Alfred P. Sloan Foundation (A.G.M.).

0006-2960/82/0421-6591$01.25/0

Since virtually all base-pair proton NMR signals from the "stem" regions of a given tRNA can be resolved at 360 MHz, proton NMR spectroscopy provides a means for monitoring (simultaneously) the unfolding of each of the four *stems* of a given tRNA (Reid, 1981). Conversely, from covalent attachment of a chemically specific nitroxide spin-label to a particular *single-stranded* nucleotide of a tRNA, changes in the rotational flexibility at specifically labeled sites on the *loops* of the tRNA can be detected from changes in the observed ESR spectrum (Dugas, 1977). A combination of the NMR and ESR (electron spin resonance) data for a given RNA should thus provide a rather detailed picture of the temperature-induced unfolding of the macromolecule (both the stems and the loops) and thus determine the stability order of the various secondary and tertiary structural segments.

ESR spin probes have proved extremely sensitive to structural differences within an RNA molecule at a given temperature, as well as to temperature-induced structural changes (Kamzolova & Postnikova, 1981). ESR spin probes have successfully demonstrated a conformational change in the anticodon following aminoacylation of tRNA (Caron & Dugas, 1976). Furthermore, Arrhenius plots of the logarithm of the rotational correlation time vs. reciprocal absolute temperature show abrupt changes in slope at temperatures coincident with the onset of "melting" of the RNA structure near the probe attachment site. From the wide variety of spin probes synthesized for attachment to various specific tRNA sites (Bobst, 1979), the temperature-induced tRNA melting of several distinct structural regions has been mapped with ESR (Dugas, 1977; Caron et al., 1976; Caron & Dugas, 1976; Weygand-Durasevic et al., 1977; Sprinzl et al., 1974; Schofield et al., 1970; Hoffman et al., 1969; Kamzolova & Postnikova, 1981).

Extension of ESR spin-labeling to *ribosomal proteins* has recently been reported (Tritton, 1978; Brakier-Gingras et al., 1978; Rodriquez & Dugas, 1981). However, interpretation of those results is complicated by possible multiple binding sites for the spin-label for even a single ribosomal protein and the lack of knowledge of the secondary structure of the labeled ribosomal proteins.

In this paper, we report the first ESR spin-labeling of ribosomal eukaryotic (*Saccharomyces cerevisiae* and wheat germ) and prokaryotic (*Escherichia coli*) 5S RNA, along with tRNA (*S. cerevisiae*) spin-labeled at the same site as a control. Specific spin-labeling at the 3′-terminal ribose of each RNA is achieved by addition of 4-amino-2,2,6,6-tetramethylpiperidinyl-1-oxy (Tempo-NH_2) to periodate-oxidized RNA as previously described for tRNA (Caron & Dugas, 1976), to give the morpholino-spin-labeled (MSL) RNA. The temperature for the onset of melting of the labeled stem region in each MSL RNA is then determined from changes in the slope of an Arrhenius plot of log (1/correlation time) vs. $1/T$ (see Theory). Finally, the potential advantages of these and other spin-labeled 5S RNAs as probes of ribosomal structure and function are discussed.

Theory

The electron spin resonance (ESR) line shapes for spin-labeled DNAs and RNAs are generally described by the "fast-motion" regime, for which the line width, $\Delta H(m_I)$, of each of the three resonance lines of a nitroxide label is given by (Goldman et al., 1972)

$$\Delta H(m_I) = A + Bm_I + Cm_I^2 \quad (1)$$

in which m_I is the ^{14}N nuclear spin z-component quantum number, A contains terms that are independent of m_I (e.g., spin–rotation)

$$B = 0.103\omega_0\left[\Delta g\Delta a\tau_0\left(1 + \frac{3}{4}\frac{1}{1+\omega_0^2\tau_0^2}\right) + 3\delta g\delta a\tau_2\left(1 + \frac{3}{4}\frac{1}{1+\omega_0^2\tau_2^2}\right)\right] \quad (2)$$

and

$$C = 1.81\times10^6\left[(\Delta a)^2\tau_0\left(1 - \frac{3}{8}\frac{1}{1+\omega_a^2\tau_0^2} - \frac{1}{8}\frac{1}{1+\omega_0^2\tau_0^2}\right) + 3(\delta a)^2\tau_2\left(1 - \frac{3}{8}\frac{1}{1+\omega_a^2\tau_2^2} - \frac{3}{8}\frac{1}{1+\omega_0^2\tau_2^2}\right)\right] \quad (3)$$

in which $\Delta a = a_z - (1/2)(a_x + a_y)$, $\delta a = (1/2)(a_x - a_y)$, $\omega_a \simeq 8.8\times10^6 a_N$, $\omega_0 = 2\pi\nu_0$, a_N is the isotropic ^{14}N hyperfine splitting, ν_0 is the ESR spectrometer frequency, a_i and g_i are hyperfine- and g-tensor components, z is the direction of the applied static magnetic field, τ_0 and τ_2 are the correlation times associated with random fluctuations in the (spherical) tensor principal components of g and a, and all terms are in units of gauss (Freed, 1976). The quantities Δg and δg are defined as for Δa and δa (Table I).

Table I

Nitroxide Spin-Label ESR Parameters

$a_{xx} = 5.9$ G	$g_{xx} = 2.0090$ G
$a_{yy} = 6.4$ G	$g_{yy} = 2.0058$ G
$a_{zz} = 38.1$ G	$g_{zz} = 2.0021$ G

Experimental Yeast MSL tRNA Parameters at 29.8 °C

$A = 1.926$ $B = -0.326$ $C = 0.353$

Additional Parameters for Simulated Spectrum of Figure 4

$R_{\|} = 3.0\times10^9$ s^{-1}
$R_{\perp} = 0.8\times10^7$ s^{-1}
$\beta = 54.3°$ = tilt angle between rotational and hyperfine axes
$a_{CH_3} = 0.17$ G
$a_{CH_2} = 0.43$ G

It is straightforward (Goldman et al., 1972) to solve eq 2 and 3 for τ_0 and τ_2 to give

$$\tau_0 = \frac{1.11\times10^{-7}}{H_0\Delta a}\frac{5\delta a - \delta g H_0 C}{\Delta g\delta a - \delta g\Delta a} \quad (4)$$

$$\tau_2 = \frac{3.69\times10^{-8}}{H_0\delta a}\frac{8\Delta g H_0 C - 5\Delta a B}{\Delta g\delta a - \delta g\Delta a} \quad (5)$$

Although τ_0 and τ_2 are needed in order to simulate the full ESR line shape (see below), simpler expressions of more practical use are obtained by rewriting eq 2 and 3 as if $\tau_0 = \tau_2 = \tau_B$ in eq 2 and $\tau_0 = \tau_2 = \tau_C$ in eq 3 to give (Polnaszek et al., 1978)

$$B = 0.103\omega_0\tau_B(\Delta g\Delta a + 3\delta a\delta g)\left(1 + \frac{3}{4}\frac{1}{1+\omega_0^2\tau_B^2}\right) \quad (6)$$

and

$$C = 1.81\times10^6\tau_C[(\Delta a)^2 + 3(\delta a)^2]\times\left(1 - \frac{3}{8}\frac{1}{1+\omega_a^2\tau_C^2} - \frac{1}{8}\frac{1}{1+\omega_0^2\tau_C^2}\right) \quad (7)$$

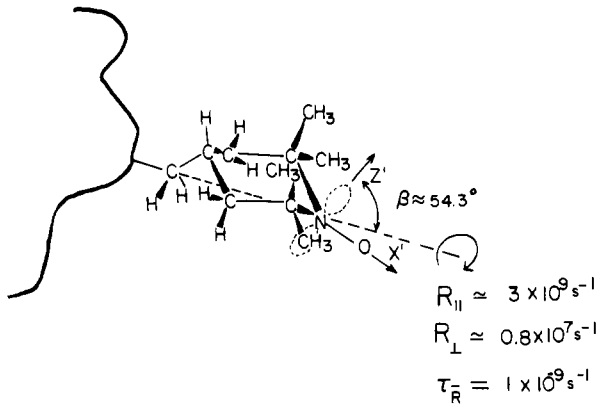

FIGURE 1: Schematic diagram of the morpholino-spin-labeled RNA 3′ terminus. The principal z axis of the rotational diffusion tensor is tilted by 54.3° with respect to the molecule-fixed hyperfine principal x' axis. $R_{\parallel}$ is the rotational diffusion tensor principal value for rotation about the z axis; $R_{\perp}$ is the value for rotation about an axis perpendicular to the z axis. τ_R is the mean correlation time for rotational diffusion (see text).

Experimental values of τ_B and τ_C are obtained from eq 6 and 7, with the values of B and C determined from the experimental peak heights ($h_{\pm 1}$, h_0) and central line widths [$\Delta H(0)$] according to

$$B = [\Delta H(0)/2][(h_0/h_1)^{1/2} - (h_0/h_{-1})^{1/2}] \quad (8)$$

$$C = [\Delta H(0)/2][(h_0/h_1)^{1/2} + (h_0/h_{-1})^{1/2} - 2] \quad (9)$$

Test for Presence of Anisotropic Rotational Motion. In the limit that the spin probe undergoes *isotropic* rotational diffusion, the characteristic times τ_B and τ_C evaluated from eq 6 and 7 will be equal, and the rotational motion is described by a *single* characteristic time, $\tau_B = \tau_C = \tau$. τ is determined from the experimental relative peak heights (h_{-1}, h_0, h_1) and central peak width [$\Delta H(0)$] from eq 10. All previous analyses

$$\tau = 6 \times 10^{-10} \Delta H(0)[(h_0/h_{-1})^{1/2} + (h_0/h_1)^{1/2} - 2] \text{ s} \quad (10)$$

of rotational lability of spin-labeled tRNA have been based on the isotropic rotational motional model of eq 10 (see Dugas, 1977).

For *anisotropic* rotational motion, $\tau_B \neq \tau_C$. When the principal rotational diffusion axis (i.e., the axis about which rotation is most rapid) is the x axis (i.e., the nitroxide N–O bond direction—see Figure 1, $\tau_B > \tau_C$. On the other hand, when the principal rotational diffusion axis is the y axis, $\tau_B < \tau_C$ (Polnaszek et al., 1978). For the present experiments, $\tau_B > \tau_C$ at most temperatures. As argued in greater detail below, the faster τ_C component is dominated by internal rotational motion, and the slower τ_B component is dominated by rotational tumbling of the labeled stem region of the RNA itself.

Absolute vs. Relative τ_B and τ_C Values. Strictly speaking, the above description applies only in the absence of unresolved proton hyperfine coupling. If the additional apparent line broadening from unresolved proton hyperfine couplings were simply included in B and C, the *absolute* apparent values of τ_B and τ_C calculated from eq 6 and 7 would be larger (i.e., longer) than the true values. Provided that such unresolved hyperfine couplings are independent of temperature (see Discussion), the systematic errors thus introduced into τ_B and τ_C will not affect conclusions about *relative* changes in τ_B and τ_C with temperature. In the present work, experimental values of h_0, h_{-1}, h_1, and $\Delta H(0)$, uncorrected for unresolved ^{1}H hyperfine splittings, are used directly to obtain τ, τ_B, and τ_C from eq 6–10.

ESR Line-Shape Simulation. In order to establish the relevance of the characteristic times τ_B and τ_C determined in the presence of inhomogeneous (unresolved proton hyperfine) broadening, it was necessary to simulate the complete ESR line *shape* (including unresolved proton hyperfine coupling) for yeast MSL-tRNA at 29.8 °C.

Simulations were based on an anisotropic rotational diffusion motional model, a computer algorithm (Polnaszek, 1976) based on the perturbation theory developed by Freed (1976) being used. The computed ESR spectrum was then convolved with the unresolved hyperfine splitting pattern for the methyl and methylene protons of the spin-label, by using a computer algorithm written for this purpose by one of us (F.G.H.). The final computed spectrum was then compared to the experimental spectrum. Finally, it is important to note that the above program permits the rotational diffusion principal axis to be tilted with respect to the z axis of the hyperfine- and g-tensor frame (see Discussion).

It is necessary to define the relations between the rotational diffusion tensor principal components, $R_{\parallel} = 1/6\tau_{\parallel}$ and $R_{\perp} = 1/6\tau_{\perp}$, and the correlation times, τ_0 and τ_2, associated with the (spherical) tensor principal components of g and A (Freed, 1976). First, if the rotational diffusion and hyperfine tensor principal axes are coincident (i.e., $R_{\parallel}$ axis along the nitroxide N–O bond), then $\tau_{\perp} = \tau_0$ for reorientation about an axis perpendicular to the nitroxide N–O bond axis. Second, the correlation time $\tau_{\parallel}$ for rotation about the symmetry axis is related to τ_2 according to (Polnaszek, 1976)

$$\tau_{\parallel} = 2\tau_0\tau_2/(3\tau_0 - \tau_2) \quad (11)$$

Finally, a convenient measure of the rotational motion of the label, averaged about all directions, is the mean correlation time

$$\tau_R = (\tau_{\parallel}\tau_{\perp})^{1/2} \quad (12)$$

Experimental Procedures

Isolation of 5S RNA and tRNA. *S. cerevisiae* cells were obtained as a gift from Carling-O'Keefe Brewery (Vancouver, B.C.). *E. coli* cells were purchased from Grain Processing Corp. (Muscatine, IA 52761). Both types of cells were stored at −20 °C. Wheat germ 5S RNA was isolated from Sigma wheat germ tRNA (G. A. Luoma and A. G. Marshall, unpublished results).

S. cerevisiae cells (220 g) were suspended in 2% sucrose solution (1700 cm^3) and stirred for ~5 h, followed by addition of an equal volume of water-saturated phenol and sodium dodecyl sulfate to a final concentration of 0.5%. The cells were then stirred overnight (~16 h) and the two phases separated by centrifugation at 10000g for 15 min. The supernatant was removed and made 0.05 M in $MgCl_2$, and the RNA was precipitated at −20 °C with 2.5 volumes of 95% ethanol.

Similarly, *E. coli* cells were suspended in 10 mM tris(hydroxymethyl)aminomethane hydrochloride (Tris-HCl) buffer, pH 7.5, containing 10 mM $MgCl_2$. An equal volume of water-saturated phenol was added and the mixture stirred for 30 min. The phases were separated by centrifugation as above, the water layer was removed, and the phenol layer was reextracted with another portion of buffer. The aqueous supernates were then combined, and the RNA was precipitated with ethanol.

All further RNA purification steps for *E. coli*, *S. cerevisiae*, and wheat germ preparations were identical. The precipitated RNA from the phenol extraction procedure was suspended in 0.3 M NaCl, the non-RNA material separated by centrifugation, and the resulting clear solution applied to a DE-32 ion-exchange column with 0.3 M NaCl (10 mM Tris, pH 7.5),

followed by elution with 1.0 M NaCl buffer and subsequent precipitation with 2.5 volumes of ethanol and 0.05 M $MgCl_2$. The precipitate was then dissolved in 1.0 M NaCl and 10 mM $MgCl_2$ and chromatographed twice on a 2 × 190 cm Sephadex G-100 gel filtration column. The isolated 5S RNAs and tRNA each exhibited a single band on 10% gel electrophoresis slabs prepared as by Rubin (1973) and showed the same relative electrophoretic mobilities as reported by Rubin. All purified RNAs were desalted on Sephadex G-25 and stored as lyophilized powders at −20 °C.

Spin-Labeling of 5S RNA and tRNA. All four tRNA species were spin-labeled with 4-amino-2,2,6,6-tetramethyl-piperidinyl-1-oxy (Tempo-NH_2), by a modified version of the procedure of Caron & Dugas (1976). A total of 2 mg of tRNA or 5S RNA was dissolved in 0.5 cm^3 of 1.0 M NaOAc buffer (pH 5.0) containing 20 mM $NaIO_4$ and stirred at 4 °C in the dark for 2 h, followed by precipitation with 2.5 volumes of ethanol at −20 °C. The precipitate was dissolved in 0.7 cm^3 of 0.2 M Na_2CO_3 buffer (pH 9.5) containing 10% dimethyl sulfoxide, and 8 mg of Tempo-NH_2 was added. The mixture was stirred at 0 °C for 90 min, followed by two additions at 30-min intervals of 45 μL of freshly prepared 0.6 M $NaBH_4$. The product was desalted on Sephadex G-25, lyophilized, and stored at −20 °C as before.

Electron Spin Resonance Spectra. Ambient-temperature spectra were recorded on a Varian E-3 ESR spectrometer. Temperature-controlled spectra were recorded on an X-band (9.0-GHz) homodyne spectrometer employing a Varian 12 in. magnet equipped with a Mark II Fieldial control. Phase-sensitive detection at 100 kHz was achieved with an Ithaco Dynatrac 391A lock-in amplifier. Field calibration was carried out by using a proton magnetometer whose resonant frequency was monitored by a Hewlett-Packard 5246L frequency counter. The same frequency counter, with a 5266 plug-in, served to measure the microwave frequency.

All temperature-controlled spectra were recorded at a 50-G spectral width, with expansion to a 10-G spectral width for measurement of the width of the central line. The temperature was determined from a thermocouple inserted into the Dewar containing the sample and was controlled by a Varian 1043 temperature control unit. Frequency modulation amplitude was set at 0.5 G, and the microwave power was kept at 5 mW to avoid saturation. All reported temperatures are accurate to within 0.5 °C.

Ambient-temperature spectra were recorded on a Varian E-3 spectrometer, at either a 50- or 100-G spectral width. The modulation amplitude was 1 G, and the microwave power was kept below 10 mW.

Samples were prepared by dissolving 1 mg of freeze-dried RNA in 50 μL of cacodylate buffer (10 mM cacodylate, pH 7.0) containing 100 mM NaCl and 10 mM $MgCl_2$. The samples were loaded into an aqueous flat cell for recording the spectra.

Pancreatic RNase Digest and Recovery of End Nucleoside. A total of 1.0 mg of RNA and 70 g of pancreatic RNase was dissolved in 0.5 cm^3 of 20 mM Tris-HCl buffer (pH 7.5) and incubated at 25 °C for 20 h. The mixture was then applied to a preequilibrated DE-32 column. The unbound fraction was eluted and collected, and the bound fraction was eluted with 0.5 M NaCl in 10 mM Tris-HCl (pH 7.5). In each case, the collected fractions were concentrated in a rotary evaporator to a final volume of about 100 μL. ESR spectra were then recorded as above, in an aqueous flat cell.

Results

Location of Spin-Label on RNA. Since the 3′-terminal ribose of each RNA is the only sugar with a 2′,3′-diol functionality (the 3′-OH is esterified to a phosphate in all the other sugars), periodate oxidation and subsequent attachment of the Tempo-NH_2 group should be specific to the 3- terminus of the RNA. So that one could prove this attachment specificity, each of three MSL RNAs after use in the temperature-denaturation studies was first chromatographed on Sephadex G-25, and the peak eluting at the void volume of the column was lyophilized and dissolved in 20 mM Tris-HCl (pH 7), and its EPR spectrum was recorded (Figure 2). The elution profiles (Figure 2, middle column) show that less than 5% of the RNA is degraded by heating, and in each case the EPR spectrum after heating and cooling (Figure 2, right) shows that the spin probe is still immobilized (compare to Figure 2, left, before heating).

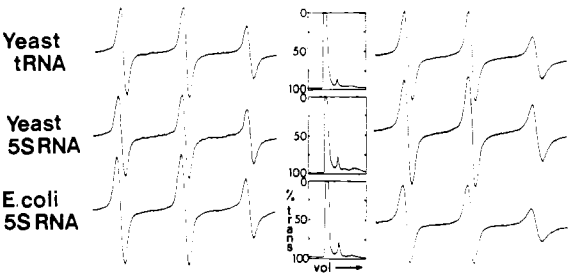

FIGURE 2: Comparison of ESR spectra of yeast MSL tRNA, yeast 5S MSL RNA, and *E. coli* 5S MSL RNA before (left) and after (right) heating to 80 °C and recooling to room temperature. The middle column shows Sephadex G-25 chromatograms after heating and recooling.

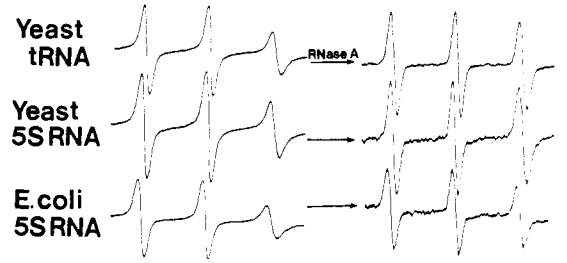

FIGURE 3: Comparison of spin-probe ESR spectrum before (left) and after (right) pancreatic RNase A digestion. For yeast 5S RNA and yeast tRNA, the right-hand spectra represent the spin-labeled 3′-terminal mononucleoside that is excluded by DE-32 ion-exchange chromatography of the digest mixture. For *E. coli* 5S RNA, the right-hand spectrum represents the terminal ApUOH dinucleotide fragment obtained by further elution from DE-32 with 0.5 M NaCl.

Each of the three RNA samples of Figure 2 was enzymatically hydrolyzed with pancreatic RNase and the digest applied to a DE-32 anion-exchange column. Since pancreatic RNase cleaves specifically on the 3′ side of pyrimidine nucleotides to leave a pyrimidine nucleoside 3′-phosphate, both *S. cerevisiae* 5S RNA and tRNA will be cleaved to produce a 3′-terminal nucleoside that *will not* bind to DE-32 (see Figure 3). On the other hand, *E. coli* 5S RNA will be cleaved to yield a 3′-terminal ApUOH dinucleotide that *will* bind to DE-32. Figure 3 shows that the DE-32 void volume fraction from hydrolyzed yeast MSL 5S RNA or MSL tRNA, when concentrated, gives an almost quantitative recovery of the spin probe, and the EPR spectral profile is characteristic of a nitroxide bound to a rapidly tumbling small molecule (i.e., a nucleoside). The void volume fraction for the *E. coli* 5S RNA, on the other hand, gave no EPR signal, but the fraction recovered after further elution with 0.5 M NaCl yielded near quantitative recovery of the spin-probe, with an EPR spectrum characteristic of a nitroxide bound to a somewhat larger molecule (i.e., a dinucleotide).

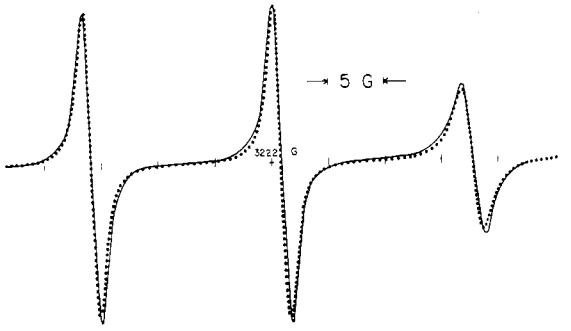

FIGURE 4: Experimental (···) and simulated (—) ESR spectra of yeast MSL tRNA at 29.8 °C. In the displayed experimental spectrum, unresolved hyperfine coupling has been removed by the Bales procedure (Bales, 1980). This simulation confirms the attachment angle for the label and the validity of the motional model from which the data of Figure 5 were produced (see Discussion).

Thermal Melting of the RNA Spin-Labeled Stem Region. Figure 5e shows an Arrhenius plot (assuming an isotropic rotational diffusion model, with a single rotational correlation time calculated from eq 8) of the present yeast MSL tRNA data, for comparison to previously reported plots for spin-labeled unfractionated *E. coli* tRNA (Caron & Dugas, 1976) and other tRNA species (Sprinzl et al., 1974; Schofield et al., 1970; Hoffman et al., 1969). For each MSL RNA, ESR spectra were recorded at several temperatures between 10 and 80 °C and rotational correlation times τ_B and τ_C computed at each temperature from experimental ESR peak heights and central peak width with eq 6–10. The resultant Arrhenius plots of $-\log \tau$ vs. $1/T$ are drawn in Figure 5a–e. These results will now be discussed, in relation to our proposed secondary structural models for eukaryotic and prokaryotic 5S RNA (Figure 6).

Discussion

(*A*) *Analysis of ESR Line Shape.* A typical experimental ESR line shape (for yeast MSL tRNA at 29.8 °C) is shown as the dotted line in Figure 4. An important feature common to all the MSL RNA spectra is the nearly equal width of the $m_I = 0$ and $m_I = 1$ lines, with a substantially broader $m_I = -1$ line. Combined with the $\tau_B > \tau_C$ result (see Theory), this feature strongly suggests anisotropic motion.

Simulated Spectrum: Coincident Diffusion and Hyperfine Tensor Axes. In order to obtain trial values for $\tau_\parallel$ and $\tau_\perp$, we begin by assuming that the rotational diffusion and hyperfine tensor principal axes are coincident (i.e., the z axis of each lies along an axis perpendicular to the nitroxide N–O bond axis, i.e., along the $2p_z$ orbital). From the experimental values of B and C of eq 2 and 3, we then compute $\tau_0 = \tau_\parallel = 5 \times 10^{-9}$ s and $\tau_2 = 1.5 \times 10^{-10}$ s, to give $\tau_\parallel = 1 \times 10^{-10}$ s from eq 11 and $\tau_R = 7 \times 10^{-10}$ s from eq 12. τ_0 thus falls just at the limit of applicability of eq 1–3. The experimentally observed ESR line-width pattern (i.e., equal widths for the $m_I = 0$ and $m_I = 1$ lines) could not be simulated with these (or any other) $\tau_\parallel$ and $\tau_\perp$ values. It was therefore concluded that the diffusion and hyperfine tensor axes are not coincident.

Simulated Spectrum: Diffusion Axes Tilted with Respect to Hyperfine Axes. The correct line-width pattern could be achieved only if the principal rotational diffusion tensor axis ($R_\parallel$) was *tilted* at an angle of 54.3 ± 0.2° with respect to the z axis of the hyperfine- and g-tensor coordinate frames. The best fit rotational diffusion constants from the simulation were $R_\parallel = 3 \times 10^9$ s^{-1} and $R_\perp = 0.8 \times 10^7$ s^{-1}, leading to $\tau_R = 1 \times 10^{-9}$ s, differing only slightly from the trial value ($\tau_R = 7 \times 10^{-10}$ s) obtained from experimental B and C values. Figure 4 shows the excellent agreement between the simulated and experimental spectra.

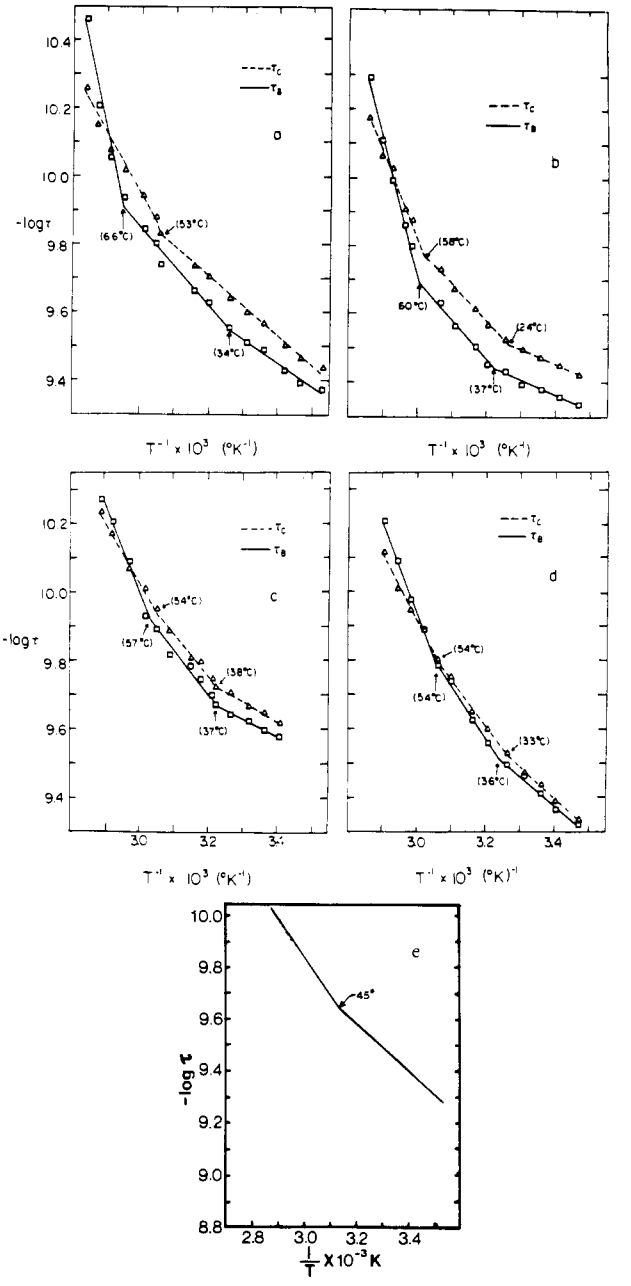

FIGURE 5: Thermal unfolding curves for five different morpholino-spin-labeled (MSL) RNAs. The Arrhenius plots are based on an anisotropic rotational diffusion model yielding two rotational correlation times (τ_B and τ_C) from the ESR spectrum at each temperature: (a) yeast MSL tRNA; (b) *E. coli* MSL 5S RNA; (c) yeast MSL 5S RNA; (d) wheat germ MSL 5S RNA; (e) yeast MSL tRNA.

Tilt Angle. The tilt angle between $R_\parallel$ and the hyperfine z axis appears very reasonable from a view of the entire spin-label molecule (Figure 1). The principal rotational diffusion axis is seen to pass directly along the long axis of the label molecule, so that rotation will be most labile about the bond between the label and the RNA. Finally, the extraordinary precision to within which the tilt angle can be determined results from the nearness of that angle to the "magic" angle, $\cos^{-1}(1/3^{1/2}) \simeq 54.74°$, about which rapid rotation averages the hyperfine interaction to 0.

Inhomogeneous Broadening Effects. All simulations were carried out by using an intrinsic line width of 0.6 G, in order to account for such effects as spin–rotation interactions.

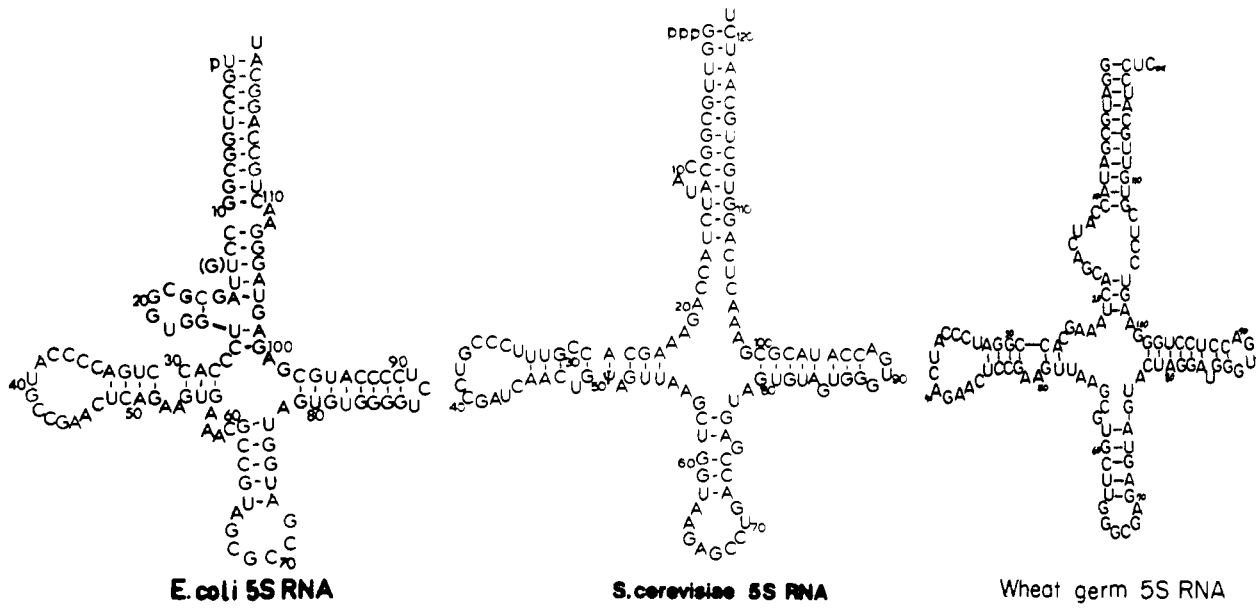

FIGURE 6: Proposed cloverleaf secondary structures for *E. coli* 5S RNA, yeast 5S RNA, and wheat germ 5S RNA (Luoma et al., 1980; Burns et al., 1980; G. A. Luoma and A. G. Marshall, unpublished results).

Additional (inhomogeneous) broadening due to unresolved proton hyperfine coupling was included by using values of 0.17 and 0.43 G for a_{CH_3} and a_{CH_2} (Polnaszek et al., 1978). In the absence of inhomogeneous broadening, the width of the simulated central ($m_I = 0$) line was 1.12 G, increasing to 1.93 G when unresolved hyperfine splittings were added, again in excellent agreement with the experimental value (1.93 G). Alternatively, the inhomogeneous broadening may be removed from the digitized experimental spectrum (Bales, 1980) to give a line width of 1.13 G, in agreement with the above 1.12-G result for the simulated spectrum.

Inhomogeneous broadening acts simply to scale the magnitude of the central line width, $\Delta H(0)$, and hence of τ_B and τ_C provided that the unresolved proton hyperfine couplings remain temperature independent. That temperature dependence can be tested by the DISPA technique (Herring et al., 1980) as follows. The dispersion vs. absorption (DISPA) plot is sensitive to all forms of inhomogeneous line broadening but is independent of homogeneous line broadening (Marshall, 1982). Thus, in the fast-motion limit, no temperature variation in the DISPA plot for the $m_I = 0$ line is expected if the unresolved proton hyperfine couplings are truly temperature independent. The result of such experiments (F. G. Herring and P. S. Phillips, unpublished results) confirm that a_{CH_3} and a_{CH_2} are indeed independent of temperature for a Tempo-type spin probe.

(*B*) *Thermal Denaturation of Spin-Labeled tRNA. Isotropic Rotational Diffusion Model.* Figure 5e shows the ESR-derived dependence of apparent *isotropic* rotational correlation time as a function of temperature (Arrhenius plots) for yeast MSL tRNA. In previous experiments, unfractionated *E. coli* tRNA was spin-labeled at the 3′-terminal ribose to give an MSL tRNA (Caron & Dugas, 1976) analogous to the present yeast MSL tRNA. Schofield et al. studied $tRNA^{Val}$ in which the α-amino group of the amino acid was spin-labeled (Schofield et al., 1970; Hoffman et al., 1969), while Sprinzl et al. linked a spin-label to a modified C_{75} nucleotide of yeast $tRNA^{Phe}$ (Sprinzl et al., 1974).

Three of the four spin-labeled tRNAs exhibit qualitatively similar behavior. Yeast MSL tRNA, SL $tRNA^{Val}$, and SL $tRNA^{Phe}$ each give Arrhenius plots with a single slope discontinuity (at 45, 47, and 51 °C, respectively), with an apparent activation energy that increases at temperatures above the reported transition, as might be expected for unfolding of the least stable segments at lower temperatures, followed by unfolding of the most stable segments at higher temperatures. We regard the present yeast MSL tRNA results as particularly reliable, since we have demonstrated the location (Figure 3) and integrity (Figure 2) of the spin-labeled moiety and shown the lack of thermal degradation of the tRNA itself (Figure 2, middle column). The *E. coli* MSL tRNA results, if correct, thus appear somewhat anomalous.

The discrepancy between the low apparent melting temperatures (45–51 °C) from the ESR experiments and the much higher melting temperatures observed in optical and NMR experiments is readily removed when the ESR spectra are analyzed with an *anisotropic* rotational diffusion model (Figure 5a).

Anisotropic Rotational Diffusion Model: Thermal Melting of Yeast MSL tRNA. Figure 5a shows Arrhenius plots for yeast MSL tRNA, on the basis of an *anisotropic* rotational diffusion model (see Theory). Although τ_B and τ_C are not related in a simple way to $\tau_\parallel$ and $\tau_\perp$, it is nevertheless accurate to say that the more rapid τ_C motion is dominated by rotation about the single bond connecting the spin-label ring to the morpholino ring bound to the amino acid acceptor stem of the tRNA (see Figure 1), while the slower τ_B motion is dominated by the slower reorientation of the stem itself. In accord with this interpretation, the data of Figure 5a show that τ_C motion is faster than τ_B motion (i.e., $\tau_C < \tau_B$) at all but the highest temperatures at which increased stem flexibility results in more isotropic rotation ($\tau_B \simeq \tau_C$). Moreover, the *internal* motion (τ_C) gives an Arrhenius plot with a single slope discontinuity, while the *stem* motion (τ_B) Arrhenius plot shows two changes in slope. Thus, an *isotropic* rotational diffusion model (Figure 5e) leads to an Arrhenius plot that reflects mainly the (less interesting) *internal* motion of the label at its site of attachment, and the (more interesting) stem flexibility of the tRNA itself is available only from the τ_B curve (Figure 5a) of the *anisotropic* motional model.

Of the four unpaired bases at the 3′ terminus of tRNA, the terminal base is probably unstacked at all temperatures (Rich & RajBhandary, 1976). The first break point (34 °C) in the τ_B Arrhenius plot of Figure 5a represents unstacking of the

three remaining unpaired bases at the 3′ terminus, and the second (66 °C) represents melting of the acceptor stem itself. The second ESR break point corresponds to the *initial* melting temperature and is thus lower than the optical T_m (~75 °C), which represents the midpoint of the stem melting. The τ_C Arrhenius plot is insensitive to unstacking of the single-stranded 3′ terminus, presumably because the spin-labeled 3′-terminal base is already unstacked at low temperature.

Anisotropic Rotational Diffusion Model: Thermal Melting of MSL 5S RNA. The τ_B Arrhenius plots for rotational diffusion in *E. coli* MSL 5S RNA, *S. cerevisiae* MSL 5S RNA, and wheat germ MSL 5S RNA (Figure 5b–d) each exhibit two "transition" temperatures as for tRNA (Figure 5a).

For each MSL 5S RNA, the lower temperature transition is due to unstacking of the single unpaired 3′-terminal spin-labeled base from the remaining stem. Further, since steric hindrance restricts internal motion for the spin-label when the 3′-terminal base is stacked, the lower temperature transition produces a break in the τ_C as well as in the τ_B plot for the MSL 5S RNAs.

The higher temperature MSL 5S RNA transition occurs for each species at the onset of unpairing of bases in the stem segment, at a temperature 6–12 °C lower than that for MSL tRNA. Thus, the stem region in the various 5S RNAs appears less rigid than in tRNA. Moreover, the transition temperature for *E. coli* MSL 5S RNA is higher (60 °C) than that for yeast (57 °C) or wheat germ (54 °C) MSL 5S RNAs. The higher rigidity for *E. coli* most likely results from the larger number of continuously paired bases (9 vs. 8) and larger number of GC pairs (5 vs. 4) in *E. coli* compared to that in yeast or wheat germ, lending further support to recently proposed secondary structural models for prokaryotic and eukaryotic 5S RNA.

Potential Uses for Spin-Labeled 5S RNA as a Probe of Ribosome Structure. The present experiments constitute the first attachment of EPR spin probes to RNA molecules that are permanent components of the ribosome. Although there have been previous reports of attachment of *protein*-specific spin probes to whole ribosomes or isolated ribosomal proteins (Tritton, 1978; Brakier-Gingras et al., 1978; Rodriguez & Dugas, 1981), interpretation of those experiments suffers from lack of knowledge of the spin probe location and of the secondary structure of the labeled protein. In contrast, the spin-labeled 5S RNA creates the possibility for observing conformational changes at the active site of the ribosome, with use of a precisely located spin probe. Although a recent experiment showed that fluorescent probes could not be attached to the 3′ terminus of 5S RNA in the *intact* 70S *E. coli* ribosome (Schreiber et al., 1979), it seems likely that the ribosome can be reconstituted with a *previously* modified 5S RNA. Experiments to test such proposals are currently in progress. Finally, nitroxide spin-labels with the chemical specificity for binding to guanine or uracil bases have been synthesized in this laboratory, for attachment to other sites on the same 5S RNA species.

Acknowledgments

We thank J. L. Smith for providing a sample of *E. coli* 5S RNA and the Carling-O'Keefe Brewery for providing *S. cerevisiae* cells. F.G.H. also thanks Carl Polnaszek for providing his computer programs.

References

Appel, B., Erdmann, V. A., Stulz, J., & Ackermann, Th. (1979) *Nucleic Acids Res. 7*, 1043–1057.

Bales, B. L. (1980) *J. Magn. Reson. 38*, 193–205.

Barber, C., & Nichols, J. L. (1978) *Can. J. Biochem. 56*, 357–364.

Bear, D. G., Schleich, T., Noller, H. F., & Garrett, R. A. (1977) *Nucleic Acids Res. 4*, 2511–2526.

Bobst, A. M. (1979) in *Spin Labeling: Theory and Applications* (Berliner, L. J., Ed.) Vol. II, pp 291–345, Academic Press, New York.

Brakier-Gingras, L., Bioleau, G., Glorieux, S., & Brisson, N. (1978) *Biochim. Biophys. Acta 521*, 413–425.

Burns, P. D., Luoma, G. A., & Marshall, A. G. (1980) *Biochem. Biophys. Res. Commun. 96*, 805–811.

Caron, M., & Dugas, H. (1976) *Nucleic Acids Res. 3*, 19–47.

Caron, M., Brisson, N., & Dugas, H. (1976) *J. Biol. Chem. 251*, 1529–1530.

Chen, M. C., Giege, R., Lord, R. C., & Rich, A. (1975) *Biochemistry 14*, 4385–4391.

Chen, M. C., Giege, R., Lord, R. C., & Rich, A. (1978) *Biochemistry 17*, 3134–3138.

Dugas, H. (1977) *Acc. Chem. Res. 10*, 47–54.

Erdmann, V. A. (1976) *Prog. Nucleic Acid Res. 18*, 45–90.

Erdmann, V. A. (1978) *Nucleic Acids Res. 5*, r1–r13.

Fiesner, D., & Maass, G. (1973) *Eur. J. Biochem. 36*, 76–88.

Fox, J. W., & Wong, K. P. (1978) *J. Biol. Chem. 253*, 18–20.

Freed, J. H. (1976) in *Spin Labelling: Theory and Applications* (Berliner, L. J., Ed.) Vol. I, pp 53–132, Academic Press, New York.

Goldman, S. A., Bruno, G. V., Polnaszek, C. F., & Freed, J. H. (1972) *J. Chem. Phys. 56*, 716–735.

Hamill, W. D., Grant, D. M., Cooper, R. B., & Harmon, S. A. (1978) *J. Am. Chem. Soc. 100*, 633–635.

Herring, F. G., Marshall, A. G., Phillips, P. S., & Roe, D. C. (1980) *J. Magn. Reson. 37*, 293–303.

Hingerty, B., Brown, R. S., & Jack, A. (1978) *J. Mol. Biol. 124*, 523–534.

Hoffman, B. M., Schofield, P., & Rich, A. (1969) *Proc. Natl. Acad. Sci. U.S.A. 62*, 1195–1202.

Holley, R. W., Apgar, J., Everett, G. A., Madison, J. T., Marquise, M., Merrill, S. H., Penswick, J. R., & Zormir, A. (1965) *Science (Washington, D.C.) 147*, 1462–1465.

Kamzolova, S. G., & Postnikova, G. B. (1981) *Q. Rev. Biophys. 14*, 223–288.

Luoma, G. A., & Marshall, A. G. (1978a) *J. Mol. Biol. 125*, 95–105.

Luoma, G. A., & Marshall, A. G. (1978b) *Proc. Natl. Acad. Sci. U.S.A. 75*, 4901–4905.

Luoma, G. A., Burns, P. D., Bruce, R. E., & Marshall, A. G. (1980) *Biochemistry 19*, 5456–5462.

Marshall, A. G. (1982) in *Fourier, Hadamard, and Hilbert Transforms in Chemistry* (Marshall, A. G., Ed.) pp 99–124, Plenum, New York.

Marshall, A. G., & Smith, J. L. (1977) *J. Am. Chem. Soc. 99*, 635–636.

Marshall, A. G., & Smith, J. L. (1980) *Biochemistry 19*, 5955–5959.

Monier, R. (1974) in *The Ribosomes* (Nomura, M., Tissieres, A., & Lengyel, P., Eds.) pp 141–168, Cold Spring Harbor Laboratory, New York.

Osterberg, R., Sjoberg, B., & Garrett, R. A. (1976) *Eur. J. Biochem. 68*, 481–487.

Polnaszek, C. F. (1976) Ph.D. Thesis, Cornell University, Ithaca, NY.

Polnaszek, C. F., Schreier, S., Butler, K. W., & Smith, I. C. P. (1978) *J. Am. Chem. Soc. 100*, 8223–8232.

Privalov, P. L., Filimonov, V. V., Benkstern, T. V., & Bayev, A. A. (1975) *J. Mol. Biol. 97*, 279-288.
Ramstein, J., & Erdmann, V. A. (1981) *Nucleic Acids Res. 9*, 4081-4084.
Reid, B. R. (1981) *Annu. Rev. Biochem. 50*, 969-996.
Rich, A., & RajBhandary, U. L. (1976) *Annu. Rev. Biochem. 45*, 805-860.
Rich, A., & Kim, S. H. (1978) *Sci. Am. 238*, 52-73.
Robertus, J. S., Lander, J. E., Finch, J. T., Rhodes, D., Brown, R. S., Clark, B. F. C., & Klug, A. (1974) *Nucleic Acids Res. 1*, 927-933.
Rodriguez, A., & Dugas, H. (1981) *Can. J. Biochem. 59*, 311-314.
Rubin, G. M. (1973) *J. Biol. Chem. 248*, 3860-3875.
Schofield, P., Hoffman, B., & Rich, A. (1970) *Biochemistry 9*, 2525-2533.
Schreiber, J. P., Hsiung, N., & Cantor, C. R. (1979) *Nucleic Acids Res. 6*, 182-193.
Sprinzl, M., Kramer, E., & Stehlik, D. (1974) *Eur. J. Biochem. 9*, 595-605.
Stultz, J., Ackermann, Th., Appel, B., & Erdmann, V. A. (1981) *Nucleic Acids Res. 9*, 3851-3861.
Swartz, U., Menzel, H. M., & Gassen, H. G. (1976) *Biochemistry 15*, 2484-2490.
Tritton, T. R. (1978) *Biochemistry 17*, 3959-3964.
Vigne, R., & Jordan, B. R. (1977) *J. Mol. Evol. 10*, 77-86.
Wagner, R., & Garrett, R. A. (1978) *Nucleic Acids Res. 5*, 4065-4075.
Weygand-Durasevic, I., Nothig-Laslo, V., Herak, J. N., & Kucan, Z. (1977) *Biochim. Biophys. Acta 479*, 332-344.
Willick, G. E., Williams, R. E., Williams, G. E., Matheson, A. T., & Sendecki, W. (1978) *FEBS Lett. 92*, 187-189.

Precision Scanning Calorimetry of Bile Salt–Phosphatidylcholine Micelles†

Charles H. Spink,‡ Karl Müller,§ and Julian M. Sturtevant*

ABSTRACT: Precision scanning calorimetry has been used to examine the thermal behavior of mixed micelles formed between bile salts and dipalmitoylphosphatidylcholine (DPPC). Complex thermal transitions are observed which change dramatically with the mole ratio of bile salt to DPPC, dilution, and ionic strength. Comparison of the behavior of sodium taurocholate (TC) mixed micelles with sodium taurodeoxycholate (TDC) mixed micelles indicates similarity in the thermal transitions at high dilution or when the actual micellar composition is similar. It was found through equilibrium dialysis that considerably less TC than TDC is incorporated into mixed micelles with DPPC at a given bile salt concentration. Accounting for these concentration differences provides a means for more direct analysis of changes in the thermal transitions with mole ratio and dilution for the two bile salt components. Resolution of the thermal transitions into several component contributions is employed as an aid to interpretation of the differential scanning calorimetry curves. The curve resolutions lead to estimates of van't Hoff and calorimetric enthalpies of the individual contributions. The results of the curve resolutions, along with the behavior of the total enthalpies of the transitions, are consistent with a transformation in micellar structure occurring when the actual micellar composition is a mole ratio of bile salt to DPPC of about 1 to 1. The transformation region is near that found from X-ray evidence and is thought to correspond to a change from disk-shaped to spherical micelles.

Bile salts are physiological detergents whose solubilizing properties are important in several fundamental biochemical processes. Through the formation of mixed micelles, bile salts render lecithin and cholesterol soluble in aqueous media, providing a mechanism for transport of these compounds from the liver to the gall bladder, and finally to the intestinal milieu (Carey & Small, 1978). The properties of mixtures of bile salts with various lipidic substances have been reviewed by Small (1971). Since a number of studies indicate that the bile salt–lecithin micellar phase may be quite complex, it seemed appropriate to apply the technique of differential scanning calorimetry (DSC)[1] to bile salt–lipid systems, using the high-sensitivity Privalov calorimeter (Privalov et al., 1975). The synthetic lecithin dipalmitoylphosphatidylcholine (DPPC) was chosen for the studies, since it has a well-defined gel to liquid-crystal transition (Mabrey & Sturtevant, 1976) at a convenient temperature. The effects of variables such as the bile salt to DPPC ratio, structure of the bile salt, counterion concentration, and dilution have been studied. As an aid to interpretation of the thermal transition curves, some equilibrium dialysis experiments were carried out with the DPPC–bile salt mixtures.

Materials and Methods

Materials. Synthetic L-α-dipalmitoylphosphatidylcholine was purchased from Calbiochem (San Diego, CA) and used

† From the Department of Chemistry, Yale University, New Haven, Connecticut 06511. *Received March 8, 1982.* This work was supported by Grants GM 04725 from the U.S. Public Health Service and PCM 7824107 from the National Science Foundation.

‡ Permanent address: Chemistry Department, State University of New York, Cortland, NY 13045.

§ Permanent address: Institut fur Röntgenfeinstrukturforschung, der Ostereichischem Akademie der Wissenschaften and des Forschungszentrums Graz, A-8010 Graz, Austria. Max Schade Foundation Fellow, 1980–1981.

[1] Abbreviations: cmc, critical micelle concentration(s); DPPC, dipalmitoylphosphatidylcholine; DSC, differential scanning calorimetry; TDC, sodium taurodeoxycholate; TC, sodium taurocholate; TLC, thin-layer chromatography.

0006-2960/82/0421-6598$01.25/0